

Supporting Information

Trimming the π Bridge of Microporous Framework for Bidentate Anchoring Polysulfides to Stabilize Lithium–Sulfur Batteries

Jie Xu, ^{a,†} Weiqiang Tang, ^{a,†} Fengtao Yu, ^b Shuangliang Zhao, ^a Dongfang Niu, ^{a,}*

Xinsheng Zhang, ^a Zhong Xin ^{a,} and Renjie Chen ^{c,*}*

^a State Key Laboratory of Chemical Engineering and School of Chemical Engineering, East China University of Science and Technology, Shanghai 200237, China

^b State Key Laboratory of Nuclear Resources and Environment School of Chemistry, Biology and Materials Science, East China University of Technology, Nanchang 330013, P. R. China

^c Beijing Key Laboratory of Environmental Science and Engineering, School of Material Science and Engineering, Beijing Institute of Technology.

*E-mail: dfniu@ecust.edu.cn;

*E-mail: xzh@ecust.edu.cn;

*E-mail: chenrj@bit.edu.cn.

† These authors contributed equally to this work.

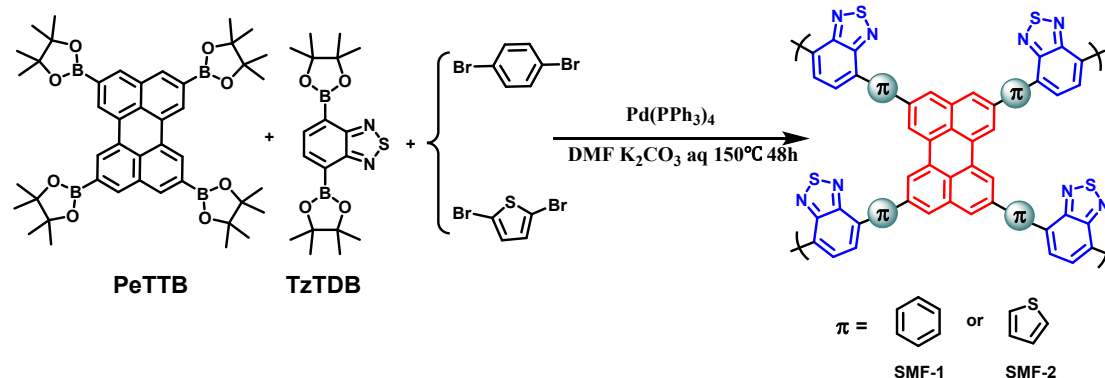
1. Preparation of SMF materials

1.1 Synthesis of the semiconducting polymers (SMF-1 and SMF-2)

General procedure for the synthesis of polymer networks: all of the target polymers were synthesized by palladium(0)-catalyzed Suzuki–Miyaura cross coupling reaction. A 100 mL Shrek tube was charged with the monomers, *N,N*-dimethylformamide (DMF), K_2CO_3 aqueous solution (2.0 M) and $Pd(PPh_3)_4$. The mixture was degassed by bubbling with N_2 for 0.5 h and heated to 150 °C for 48 h. The mixture was cooled to RT and poured into water. The precipitate was collected by filtration and washed multiple times with H_2O , THF and methanol, respectively. Further purification of the polymers was carried out by Soxhlet extraction with THF for 48 h and the product was dried under reduced pressure.

Synthesis of SMF-1: PeTTB (680.8 mg, 0.9 mmol), 4,7-bis(4,4,5,5-tetramethyl-1,3,2-dioxaborolan-2-yl)benzo[*c*][1,2,5]thiadiazole (77.6 mg, 0.2 mmol), 1,4-dibromobenzene (471.8 mg, 2 mmol), $Pd(PPh_3)_4$ (10 mg, 8.6 μ mol), 2 mL K_2CO_3 aq and 10 mL DMF were used in this polymerization. After work-up and Soxhlet extraction, a red powder **SMF-1** (357 mg, 92%) was afforded.

Synthesis of SMF-2: TzTDB (680.8 mg, 0.9 mmol), 4,7-bis(4,4,5,5-tetramethyl-1,3,2-dioxaborolan-2-yl)benzo[*c*][1,2,5]thiadiazole (77.6 mg, 0.2 mmol), 2,5-dibromothiophene (483.9 mg, 2 mmol), $Pd(PPh_3)_4$ (10 mg, 8.6 μ mol), 2 mL K_2CO_3 aq and 10 mL DMF were used in this polymerization. After work-up and Soxhlet extraction, a dark red powder **SMF-2** (421 mg, 90%) was afforded.



Scheme S1. General synthetic route of **SMF-1** and **SMF-2**.

1.2 Materials characterization

^1H and ^{13}C NMR spectra were obtained in deuterated solvents on Bruker AM-400 MHz with tetramethylsilane (TMS) as an internal standard. High-resolution mass spectra (HRMS) measurements were performed using a Waters LCT Premier XE spectrometer. Thermo gravimetric analyzer (TGA) measurement of the polymers was performed using a TA Q600 instrument under N_2 flow. The Fourier transform infrared (FT-IR) spectra was recorded on NICOLET 380 spectrometer using a standard KBr pellet technique in the frequency range of $4000\text{--}400\text{ cm}^{-1}$. Powder X-ray diffraction (PXRD) patterns was obtained on a RigakuD/MAX 2550 diffract meter (Cu K radiation, $\lambda = 1.5406\text{ \AA}$), operated at 40 kV and 100 mA. Contact angle was recorded by a DataPhysics OCA-30 instrument. Transmission electron microscopy (TEM) images and energy dispersive spectrum (EDS) were taken by JEOL JEM-2100 operating at 200 kV. XPS data were obtained on a Perkin-Elmer PHI 5000C ESCA system with Al $\text{K}\alpha$ radiation operated at 250 W. All binding energies were referenced to the C 1s peak at 284.6 eV. Surface areas and pore size distributions were measured by N_2 adsorption and desorption at 77.3 K using an ASAP 2420-4 (Micromeritics) volumetric adsorption analyzer. Surface area was calculated in the relative pressure (P/P_0) ranging from 0.05 to 0.20. Pore size distributions and pore volumes were derived from the N_2 adsorption branch using non-local density functional theory (NL-DFT). Powder samples were degassed offline at $120\text{ }^\circ\text{C}$ for 12 h under dynamic vacuum (10^{-5} bar) before analysis. Zeta potential measurements were performed in a Zetasizer Nano ZS (Malvern Instruments Ltd.) at room temperature.

2. Supporting figures

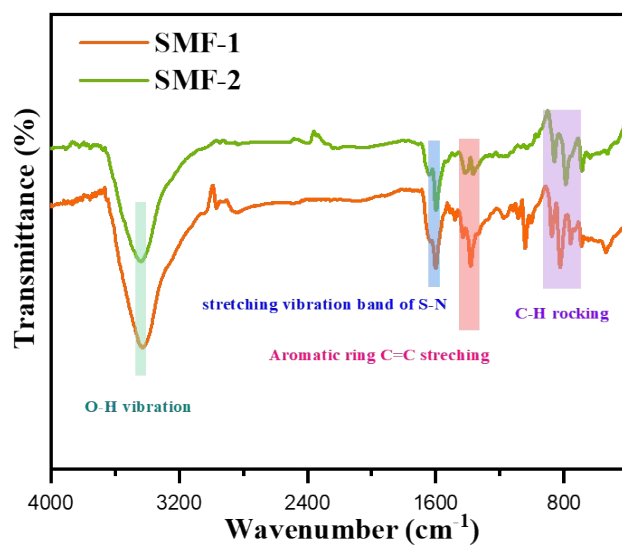


Figure S1. FT-IR spectroscopy of SMF-1 and SMF-2.

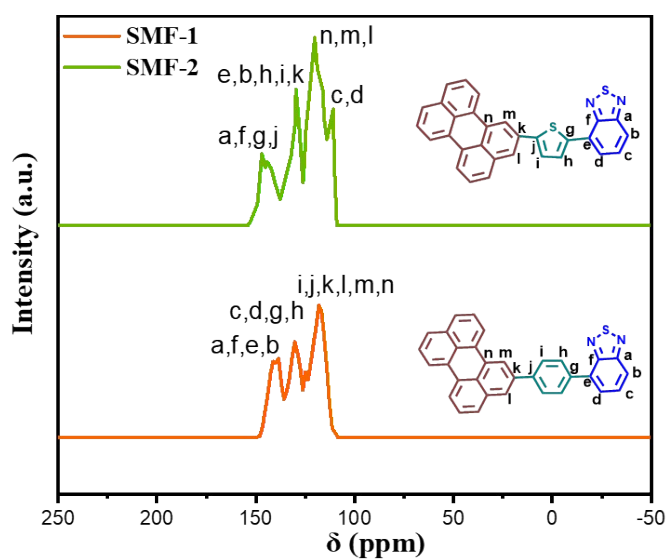


Figure S2. Solid-state ^{13}C CP-MAS NMR spectra of SMF-1 and SMF-2.

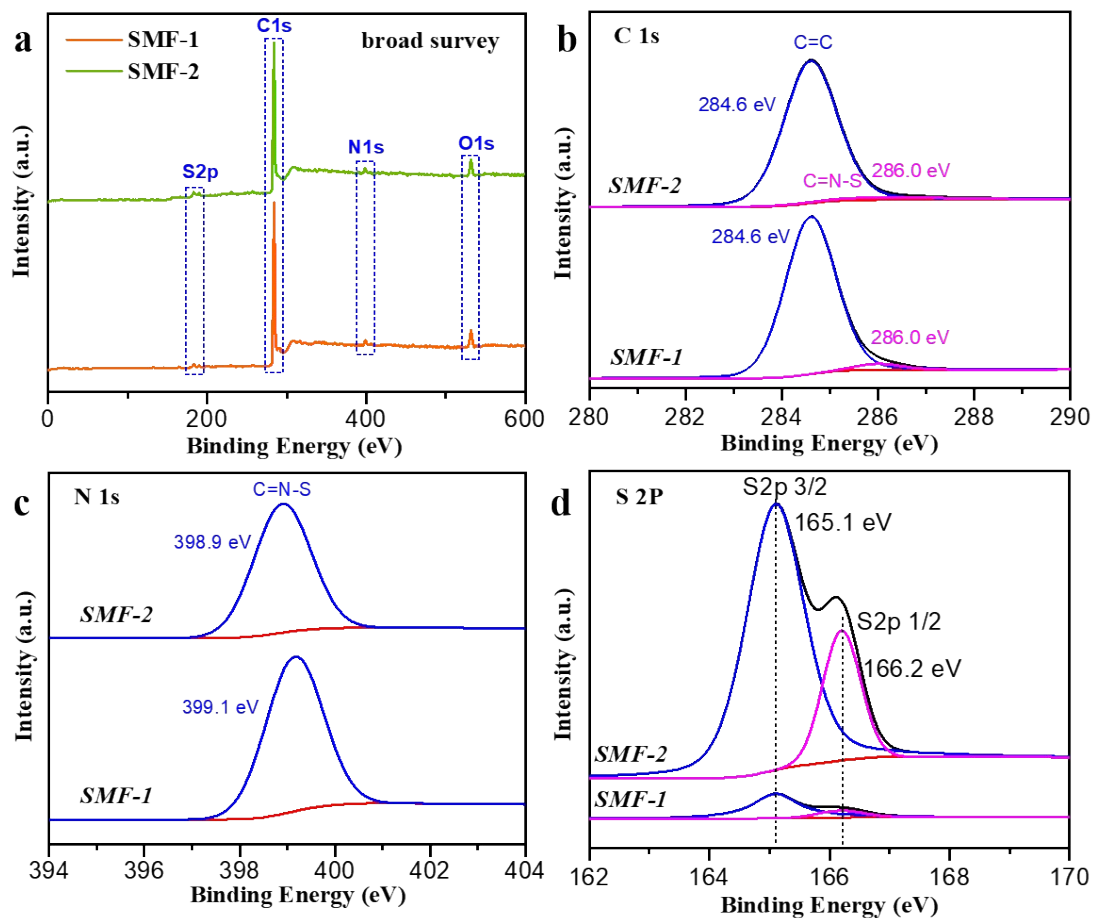


Figure S3. XPS survey with the broad survey and the fine spectra of C 1s, N 1s and S 2p, respectively.

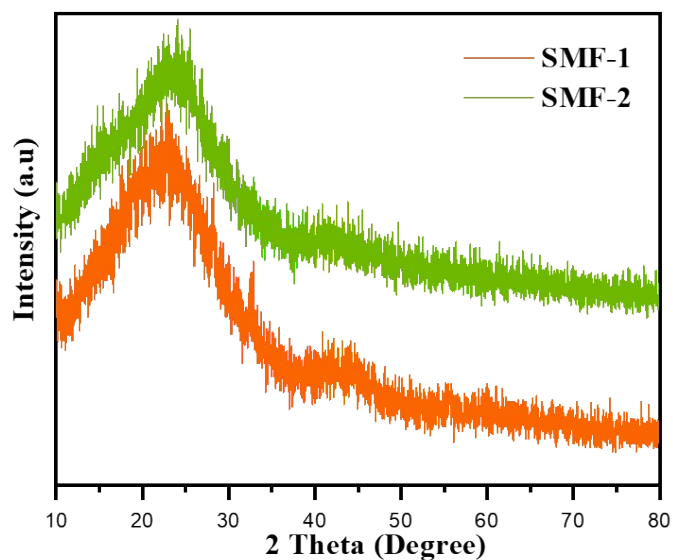


Figure S4. The powder X-ray diffraction (PXRD) signals of SMF materials.

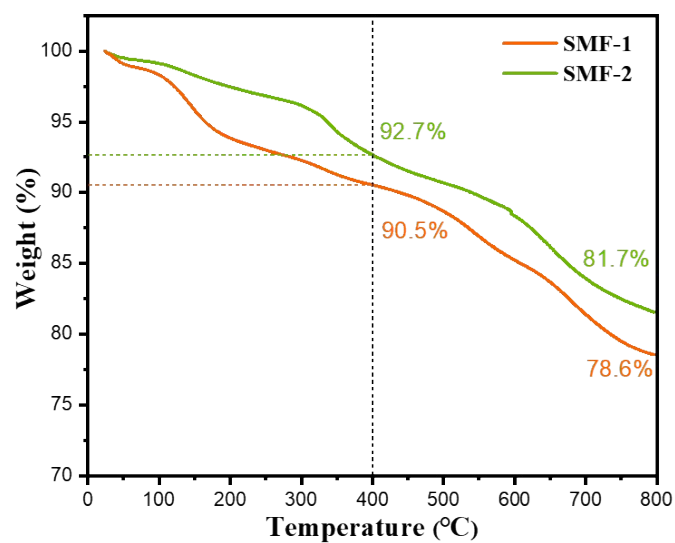


Figure S5. TGA traces for SMF-1 and SMF-2 under the nitrogen atmosphere.

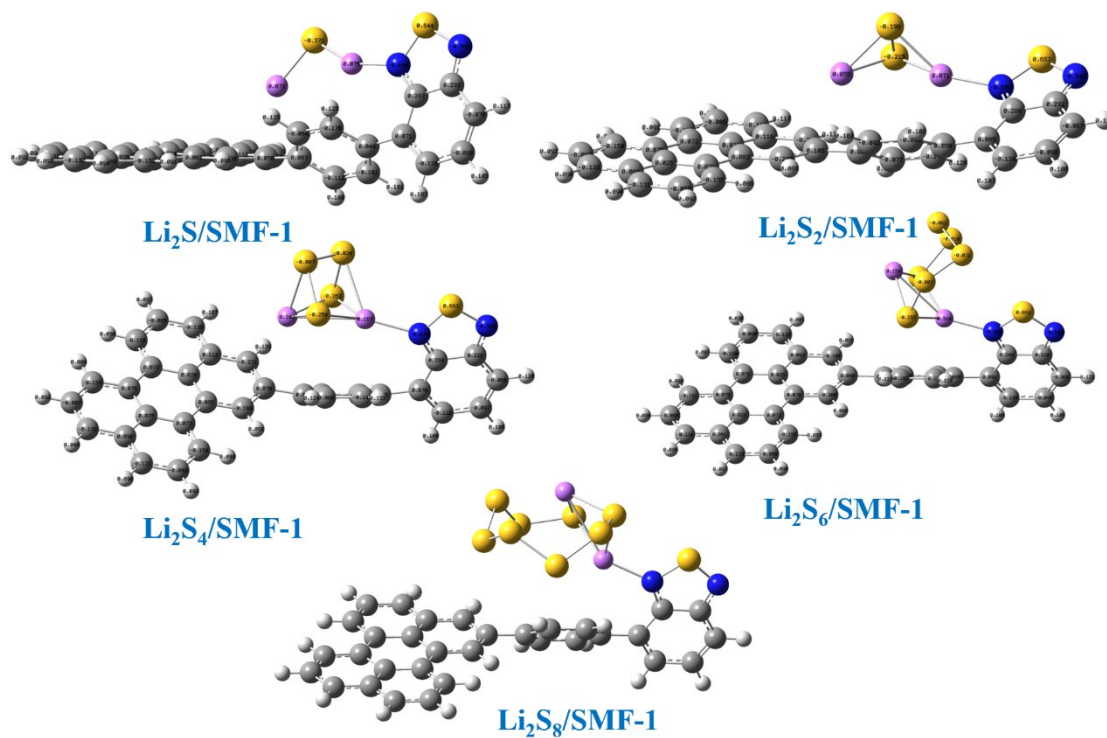


Figure S6. Equilibrium binding structures of SMF-1 towards lithium polysulfides.

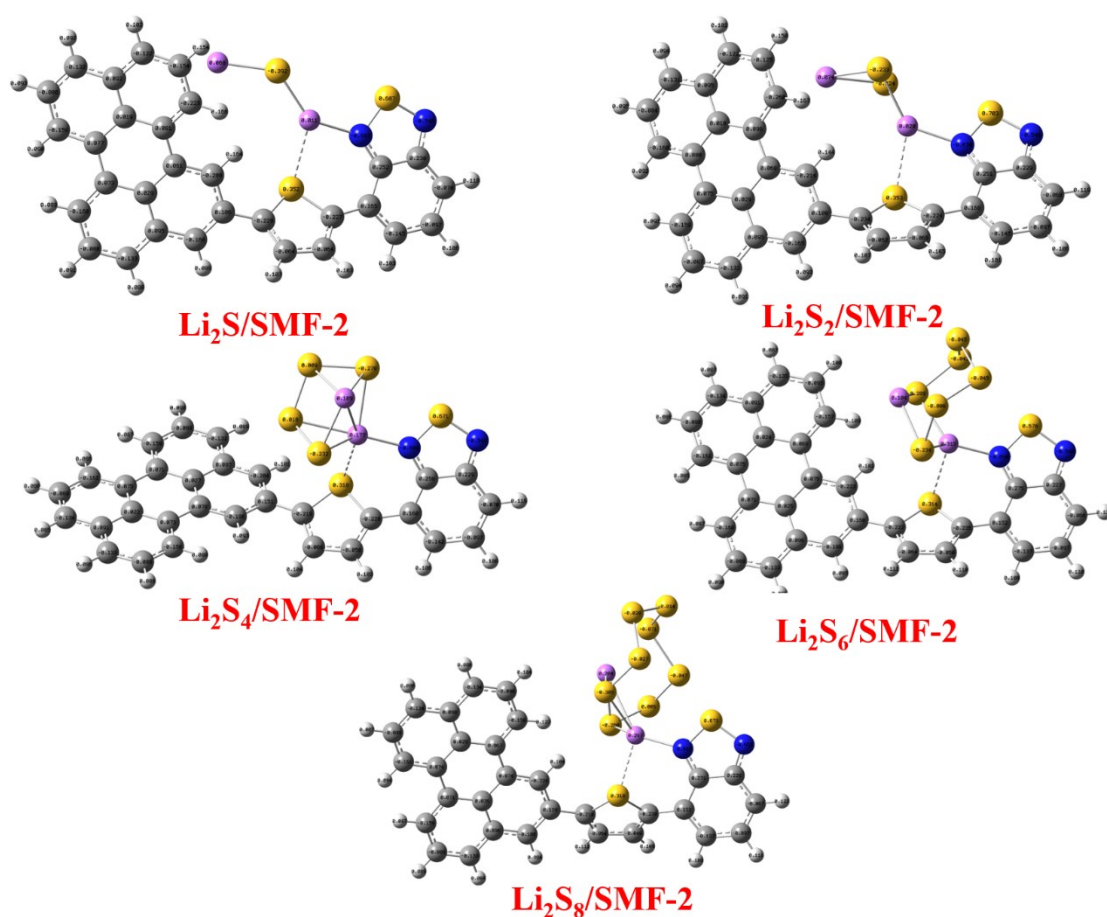


Figure S7. Equilibrium binding structures of SMF-2 towards lithium polysulfides.

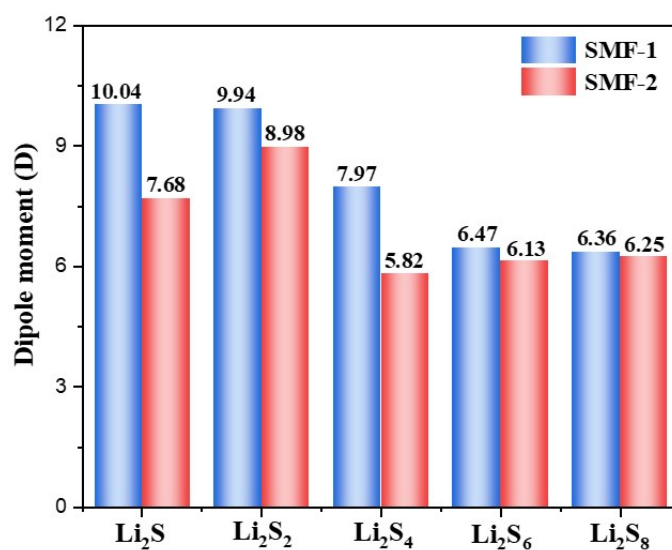


Figure S8. Dipole moment values of Li₂S_x/SMF-1 and Li₂S_x/SMF-2 complexes, respectively.

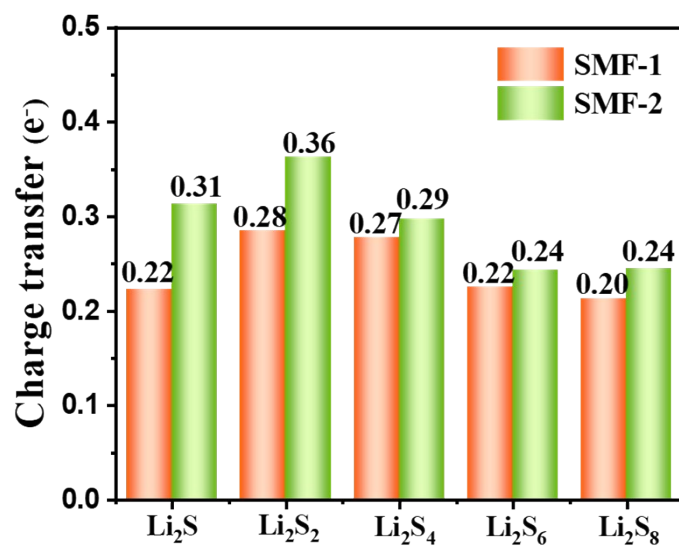


Figure S9. Calculated CT values between SMF and various LiPSs.

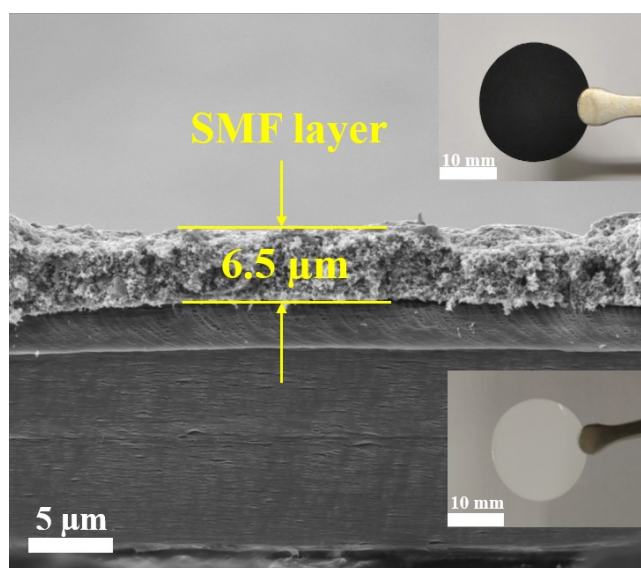


Figure S10. Cross-sectional image of the thin SMF coating layer on Celgard.

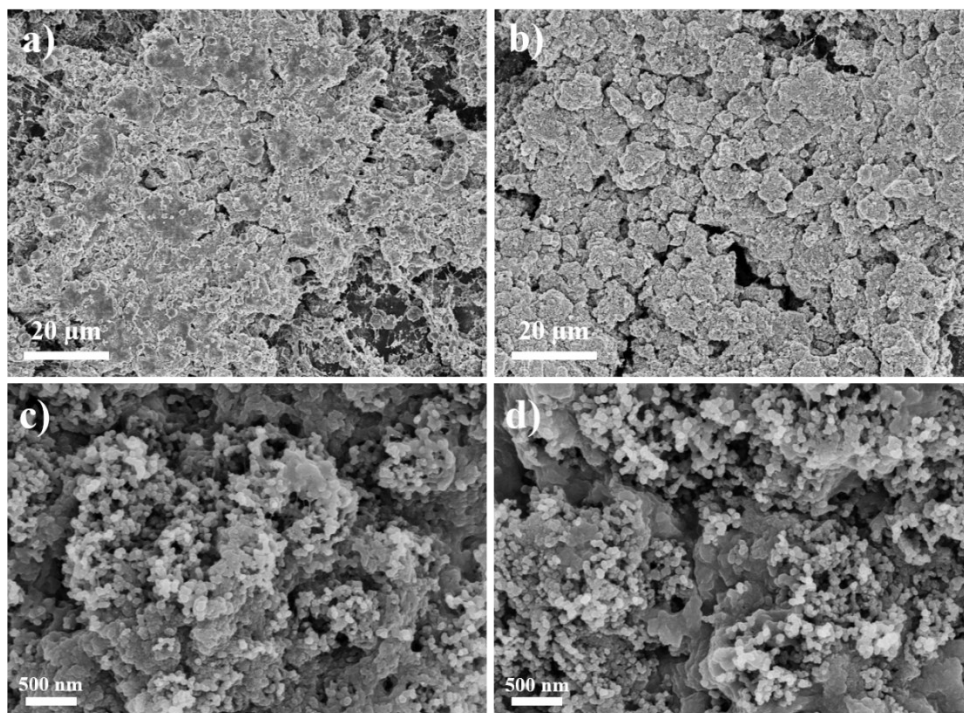


Figure S11. Top-view SEM images of SMF-1 (a,c) and SMF-2 (b,d) coating layers, respectively.



Figure S12. Digital images of SMF modified separators before folding (a), folding (b) and after folding (c), respectively.

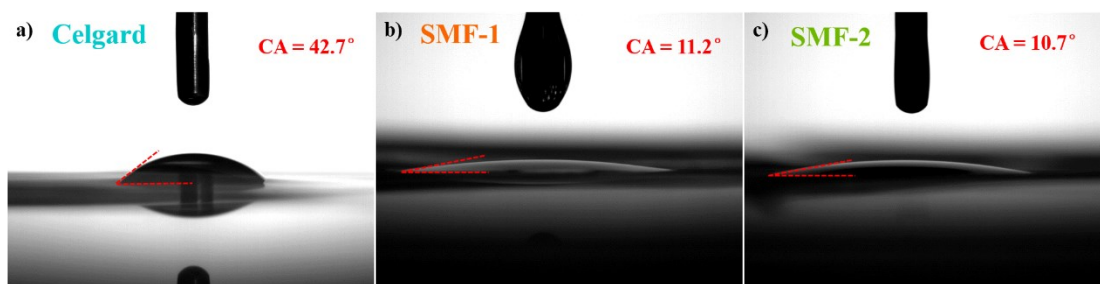


Figure S13. Contact angel images of pristine Celgard separator (a), SMF-1 coating separator (b), and SMF-2 coating separator (c), respectively.

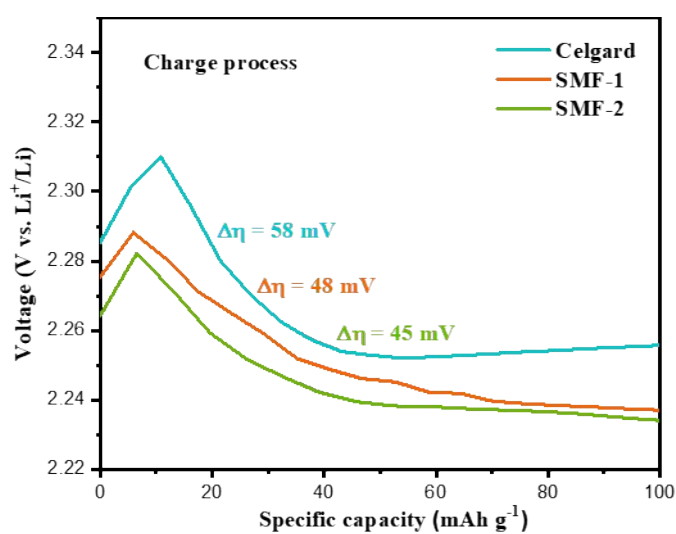


Figure S14. Charge profiles of the cells with Celgard, SMF-1 and SMF-2 modified separators showing the overpotentials for conversion between insoluble $\text{Li}_2\text{S}_2/\text{Li}_2\text{S}$ and soluble LiPSs.

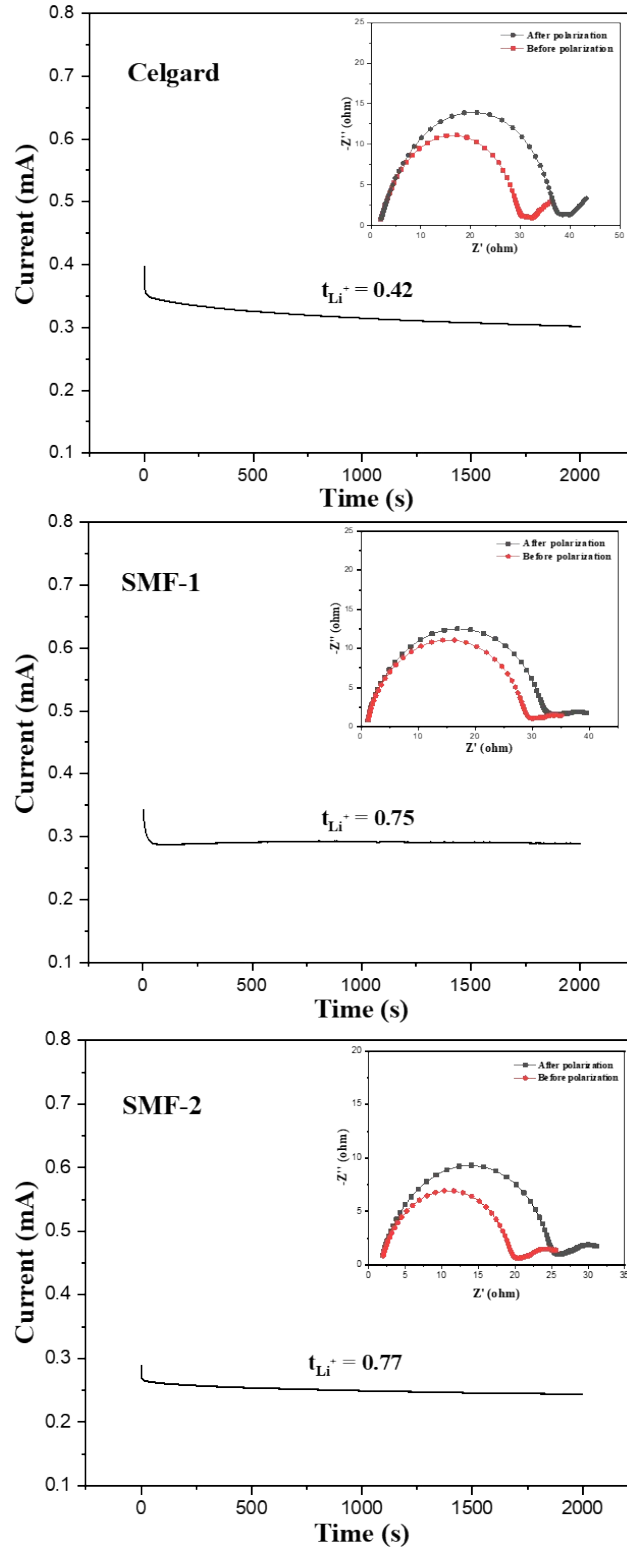


Figure S15. The time-dependence response of potentiostatic DC polarization for Li-Li symmetric cells with Celgard separator, SMF-1, SMF-2 modified separators, respectively, the inserts are the Nyquist plots of tested cells before/after polarization at room temperature.

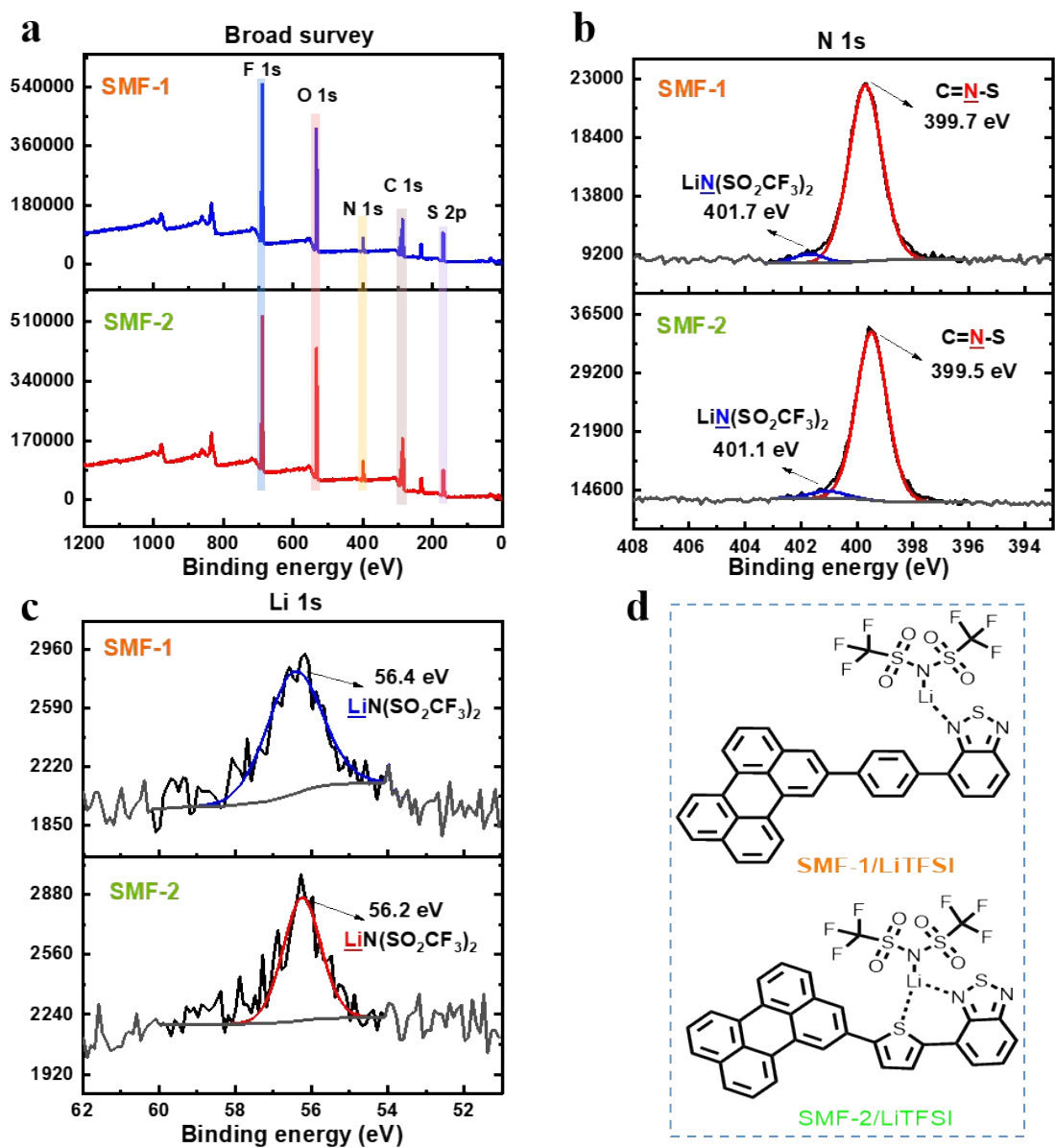


Figure S16. XPS surveys with broad survey (a), N 1s fine spectrum (b), Li 1s fine spectrum (c) of electrolyte-soaked SMFs; (d) proposed binding mechanism between SMFs and LiTFSI.

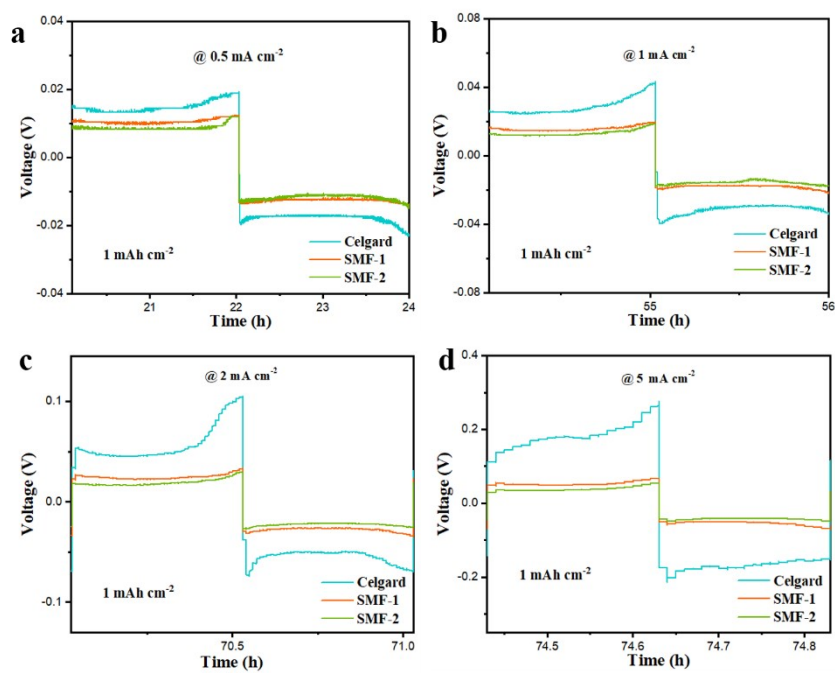


Figure S17. Polarizing voltage magnification pictures of Li||Li symmetric cells under different current rate. (Related to Fig. 3a)

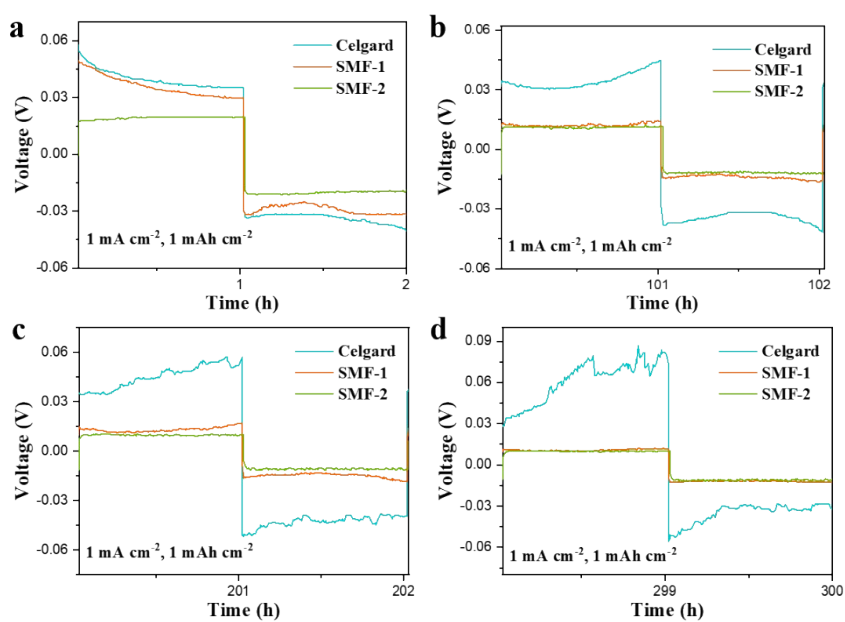


Figure S18. Polarizing voltage magnification pictures of Li||Li symmetric cells under various cycling at the current density of 1 mA cm^{-2} . (Related to Fig. 3b)

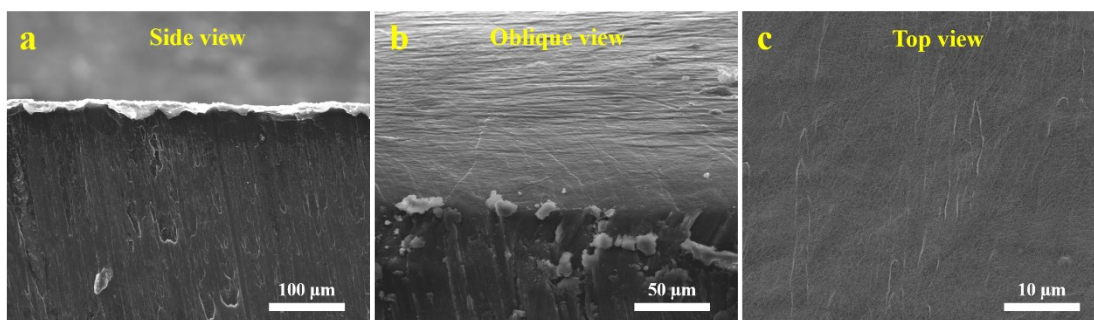


Figure S19. SEM images of pristine Li foil with side (a), oblique (b) and top (c) views, respectively.

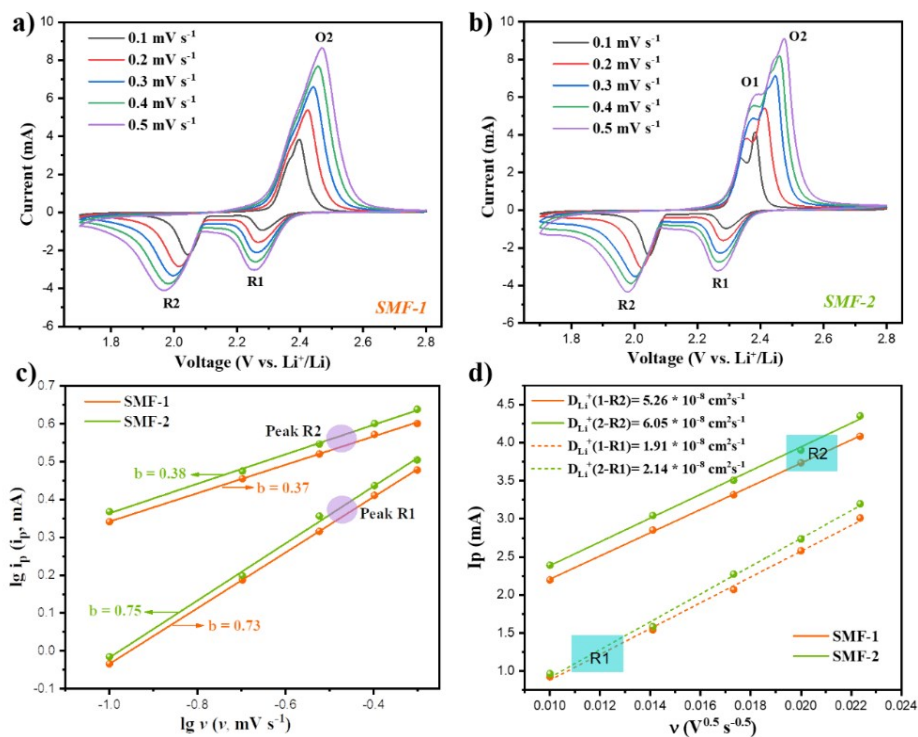


Figure S20. CV curves for SMF-1 (a) and SMF-2 (b) and b-value plots (c) as well as D_{Li^+} plots (d) at different sweep rates, respectively.

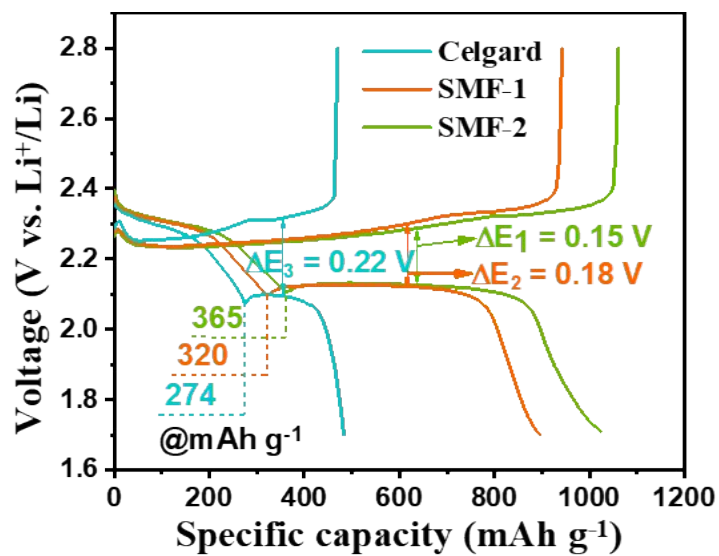


Figure S21. Initial discharge-charge voltage profiles with SMF modified separators and routine Celgard under the current of 0.2 C.

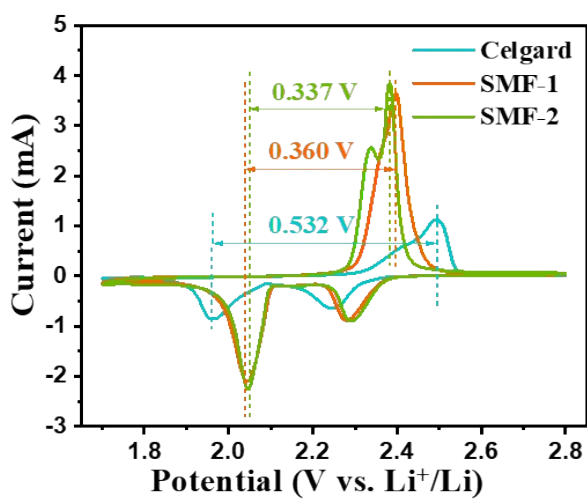


Figure S22. CV curves of the cells with various separators with the scan rate of 0.1 mV s⁻¹.

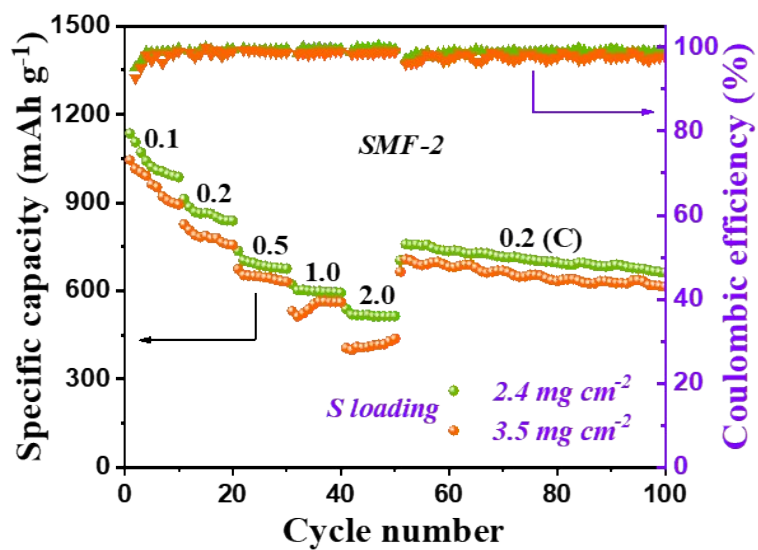


Figure S23. Rate performances with SMF-2 separator under the sulfur loading of 2.4 and 3.5 mg cm⁻², respectively.

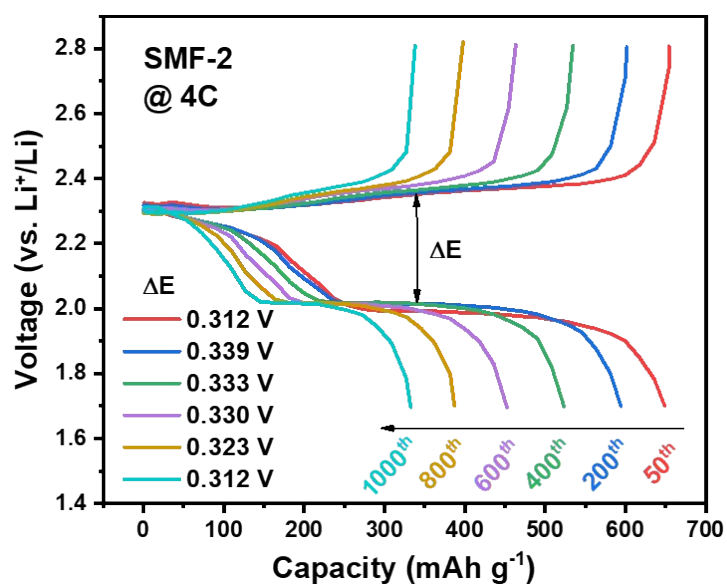


Figure S24. The discharge/charge voltage profiles of SMF-2 modified cell at the current density of 4C (the voltage gap (ΔE) was calculated at the point of half discharge capacity).

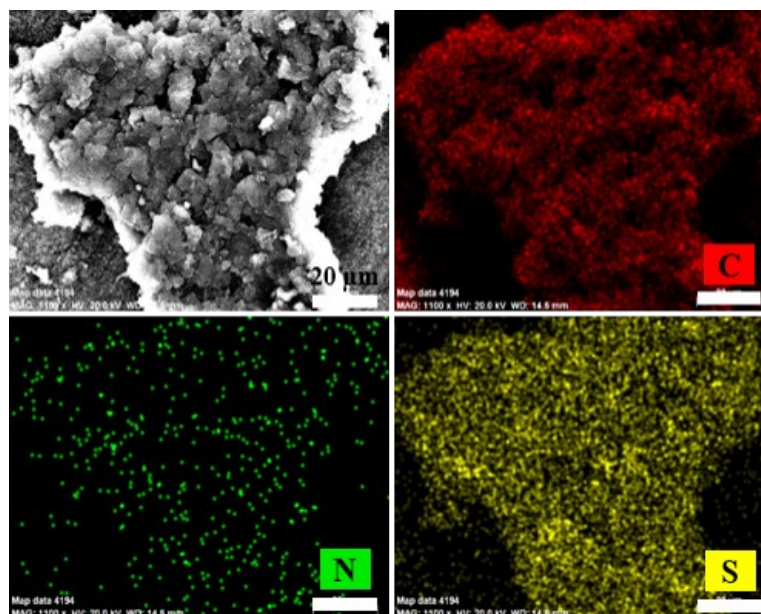


Figure S25. Elemental mapping images of SMF-2 modified separator after cycling.

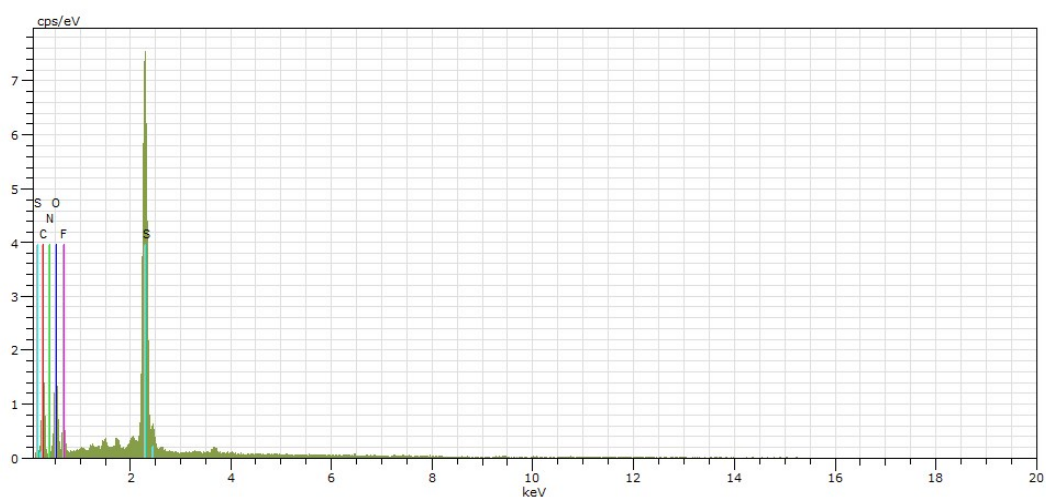


Figure S26. EDX spectrum of the SMF-2 modified separator after cycling.

3. Supporting tables

Table S1. Elemental composition (atom ratios) of samples according to XPS analysis

Sample	C/at %	N/at %	O/at %	S/at %
SMF-1	90.5	1.9	6.0	1.6
SMF-2	87.5	1.5	4.9	6.1

Table S2. Relative ratios of two carbon species determined by C 1s spectra for samples

Sample	C=C			C=N-S		
	Binding	area	%	Binding	area	%
	Energy(eV)			Energy(eV)		
SMF-1	284.6	32637.6	96.7	286.0	1099.0	3.2
SMF-2	284.6	31892.6	96.2	286.0	1245.3	3.8

Table S3. Summary of pore properties for the SMF-1 and SMF-2

Sample	$S_{\text{BET}}^{\text{a}}$	$S_{\text{Micro}}^{\text{b}}$	$V_{\text{Micro}}^{\text{c}}$	$V_{\text{Total}}^{\text{d}}$	$S_{\text{Micro}}/S_{\text{BET}}$	$V_{\text{Micro}}/V_{\text{Total}}$
	($\text{m}^2 \text{g}^{-1}$)	($\text{m}^2 \text{g}^{-1}$)	($\text{m}^3 \text{g}^{-1}$)	($\text{m}^3 \text{g}^{-1}$)	(%)	(%)
SMF-1	870.2	626.5	0.35	0.56	72	62.5
SMF-2	964.7	781.4	0.40	0.62	81	64.5

a. Surface area was calculated from N_2 adsorption isotherm in the relative pressure (P/P_0) range from 0.05 to 0.20;

b. Micropore surface area calculated from the N_2 adsorption isotherm using t-plot method based on the Harkins Jura equation;

c. Micropore volume derived from the t-plot method;

d. Total pore volume at $P/P_0 = 0.90$.

Table S4. Bond length analysis between SMF structure and the terminal Li of LiPSs

LiPSs	SMF-1: Li-N (\AA)	SMF-2: Li-N (\AA)	SMF-2: Li-S (\AA)
Li_2S	2.071	2.051	2.546
Li_2S_2	2.068	2.047	2.561
Li_2S_4	2.091	2.073	2.716
Li_2S_6	2.062	2.057	2.667
Li_2S_8	2.049	2.046	2.671
Average	2.068	2.055	2.632

Table S5. EIS test results of the cells with various separators

Sample	R_s/Ω	R_{ct}/Ω
Celgard	4.1	83
SMF-1	4.0	34
SMF-2	3.6	27

Table S6. Comparison of the electrochemical performance between SMF-2 and other polymers in the applications of sulfur host or coating layer (12 examples in recent 3 years).

Separator	Sulfur loading (mg cm^{-2})	Sulfur content	Cathode	Discharge Capacity	Publish Year	Ref.
Celgard-2400	1.4	46.2%	NPGO/S	605 mAh g^{-1} , 500 th , 1.0 C	2017	S1
Celgard-2400	0.7	51.6%	SF-CTF-1	1138 mAh g^{-1} , 1 st , 0.05 C	2017	S2
Celgard-2300	1.2	36.6%	TPE-IEMPO-S	900 mAh g^{-1} , 1 st , 0.1 C	2017	S3
Y-FTZB	1.0	70%	sulfur	1101 mAh g^{-1} , 1 st , 0.1 C	2017	S4
Celgard-2400	0.75	49%	UHCS-900	1200 mAh g^{-1} , 1 st , 0.1 C	2017	S5
Celgard-2400	0.8-2.0	49%	Py-COF/S	960 mAh g^{-1} , 1 st , 0.5 C	2018	S6
PB/Celgard	N/A	60%	KB/sulfur	984 mAh g^{-1} , 1 st , 0.2 C	2018	S7
Celgard-2400	1.1	58%	S/POF/CB	1100 mAh g^{-1} , 1 st , 0.2 C	2018	S8
ZBCP/CNT/GF	1.0	70%	S/super P	738 mAh g^{-1} , 200 th , 0.25C	2018	S9
Celgard	N/A	<60%	PS@TFPPy-ETTA-COF	698 mAh g^{-1} , 1 st , 0.2C	2019	S10
Celgard-2400	1.0	71.3%	S-COP-99	1050.2 mAh g^{-1} , 1 st , 0.1C	2019	S11
Celgard	N/A	45%	LPS-MOFs/S	835 mAh g^{-1} , 200 th , 0.1C	2019	S12
SMF-2	1.5	75%	S/CB	1149 mAh g^{-1}, 1st, 0.1 C 814 mAh g^{-1}, 200th, 0.2 C 565 mAh g^{-1}, 1000th, 1.0 C	-	this work

4. Supporting references

- [S1] C.-Y. Chen, H.-J. Peng, T.-Z. Hou, P.-Y. Zhai, B.-Q. Li, C. Tang, W. Zhu, J.-Q. Huang, Q. Zhang, *Adv. Mater.* **2017**, *29*, 1606802.
- [S2] S. H. Je, H. J. Kim, J. Kim, J. W. Choi, A. Coskun, *Adv. Funct. Mater.* **2017**, *5*, 1703947.
- [S3] B. Zhou, X. Hu, G. Zeng, S. Li, Z. Wen, L. Chen, *ChemSusChem* **2017**, *10*, 2955.
- [S4] M. Li, Y. Wan, J. Huang, A. H. Assen, C. Hsiung, H. Jiang, Y. Han, M. Eddaoudi, Z. Lai, J. Ming, L. J. Li, *ACS Energy Lett.* **2017**, *2*, 2362.
- [S5] G.-P. Hao, C. Tang, E. Zhang, P. Zhai, J. Yin, W. Zhu, Q. Zhang, S. Kaskel, *Adv. Mater.* **2017**, *29*, 1702829.
- [S6] Y. Meng, G. Lin, H. Ding, H. Liao, C. Wang, *J. Mater. Chem. A* **2018**, *6*, 17186.
- [S7] X. Wu, L. Fan, Y. Qiu, M. Wang, J. Cheng, B. Guan, Z. Guo, N. Zhang, K. Sun, *ChemSusChem* **2018**, *11*, 3345.
- [S8] B.-Q. Li, S.-Y. Zhang, L. Kong, H.-J. Peng, Q. Zhang, *Adv. Mater.* **2018**, *30*, 1707483.
- [S9] J.-K. Huang, M. Li, Y. Wan, S. Dey, M. Ostwal, D. Zhang, C.-W. Yang, C.-J. Su, U.-S. Jeng, J. Ming, A. Amassian, Z. Lai, Y. Han, S. Li, L.-J. Li, *ACS Nano* **2018**, *12*, 836.
- [S10] F. Xu, S. Yang, X. Chen, Q. Liu, H. Li, H. Wang, B. Wei, D. Jiang, *Chem. Sci.* **2019**, *10*, 6001.
- [S11] H. Shin, D. Kim, H. J. Kim, J. Kim, K. Char, C. T. Yavuz, J. W. Choi, *Chem. Mater.* **2019**, *31*, 7910.
- [S12] A. E. Baumann, X. Han, M. M. Butala, V. S. Thoi, *J. Am. Chem. Soc.* **2019**, *141*, 17891.